International Journal of Environmental Sciences
ISSN: 2229-7359
Vol. 11 No. 18s, 2025
https://theaspd.com/index.php

Studies Of Gas Sensing Behaviour And Biological Application For Ceria, Titania And Mixed Oxides Of Ce And Ti

Gomuraj Santhanaraj[1,2]**Mathavan Alagarsamy**[1]
[1]Department of Chemistry, V.O.Chidambaram College, Thoothukudi- 628 008, Tamil Nadu, India.
[2]Research Scholar, Registration No.17212232031002, Department of Chemistry, V.O.Chidambaram College, Thoothukudi, Affiliated to Manonmaniam Sundaranar University, Abishekapatti, Tirunelveli-627 012, Tamil Nadu, India.

Abstract:
Conserving energy and the environment depends significantly on the detection and monitoring of exhaust and toxic gases. Affordable, low-power gas sensors are highly looked after. Because of their great sensitivity and selectivity, metal oxide gas sensors are becoming more and more widely recognized. This research work discusses a fictional attempt to synthesize and characterize metal oxides, specifically titanium oxide, cerium oxide, and a combination of cerium and titanium mixed metal oxide known as CTMMO. The co-precipitation method with a microwave reaction system is employed for nanoparticle preparation, and various analytical techniques, such as FT-IR, UV-VIS(DRS), FE-SEM, EDAX, AFM, and XRD analysis, are utilized to characterize the prepared nanoparticles. The FT-IR spectrum of CTMMO indicates the formation of mixed metal oxide of cerium and titanium. The XRD pattern confirmed the cubic fluorite structure of CeO_2. In this research work, the voltammetric studies were carried out at Ph 7.00 buffer solution using glassy carbon electrode to explore the use of titanium oxide, cerium oxide, and cerium titanium mixed metal oxides (CTMMO) in sensing of ammonia and hydrogen sulfide at the scan rate of 20 mV/s. The binding interaction studies of ovalbumin the protein was explored by using UV-visible absorption and fluorescence spectral methods. The impressive antibacterial properties of metal oxides and mixed metal oxides were studied against the different bacteria's using the disc diffusion method.
Keywords: *anti-bacterial characteristics, cerium oxide, FE-SEM, mixed metal oxides and titanium oxide.*

INTRODUCTION:

Metal oxide nanoparticles possess remarkable properties that set them apart from conventional materials.[1] Their small size, grants them unique physical and chemical characteristics. Due to their high surface area to volume ratio, these metal oxide nanoparticles exhibit enhanced reactivity, making them highly effective in a variety of applications.[2]

Mixed metal oxides, a subset of metal oxides, are compounds formed by combining two or more different metallic elements with oxygen.[3] This blending creates hybrid compounds that offer a unique combination of properties, surpassing those of individual metal oxides. These oxide materials offer unique properties that are distinct from their constituent metals. The synthesis of mixed metal oxides often involves carefully controlling the composition and structure of the material. By selecting specific combinations of metal cations, researchers can tune the properties of the oxide to suit specific needs. Metal oxides and mixed metal oxides are fascinating materials with a vast array of applications.[4] The numerous methods have been documented in the recent reviews for the synthesis of a broad range of metal oxide and mixed oxide NPs.[5] Among them, microwave-assisted co-precipitation method have fascinated many researchers in contemporary science owing to the advantages of the purity and homogeneity of the synthesize product, energy efficient, rapid formation of product and preparation of nanosized inorganic material. The microwave-assisted co-precipitation method is a process wherein nanoparticles are synthesized by co-precipitating metal ions in the presence of microwave irradiation.[6] By applying microwave energy, the reaction kinetics are accelerated, resulting in a rapid formation of nanoparticles. This technique offers several advantages over conventional methods, including reduced reaction time, improved homogeneity, and enhanced control over particle size and morphology. In fact, particle sizes, surface areas and mechanical properties of the materials obtained by these methods can be changed according to the temperature, operating conditions, and to the used precursor.[7]

Among the different types of metal oxides, titanium oxide (TiO_2) and cerium oxide (CeO_2) have gained significant attention due to their remarkable properties and versatile applications. Titanium oxide and

cerium oxide are essential metal oxides that have revolutionized numerous applications in industries.[8] Titanium dioxide, also known as titanium (IV) oxide or titania, is a versatile white pigment that has gained immense popularity and widespread use in various applications. It exists in three main crystalline forms: rutile, anatase, and brookite. These different crystal structures give rise to varying properties, making titanium oxide a versatile material. It exhibits excellent photocatalytic properties, high refractive index, UV-visible absorption, Chemical stability making it a popular choice in the various field. It is extensively used in the manufacturing of self-cleaning glass, air and water purification systems, and even in the removal of pollutants from wastewater.[9] Furthermore, titanium oxide finds extensive applications in the cosmetics industry. It is a key ingredient in sunscreens, as it provides protection against harmful UV radiation by scattering and absorbing the UV rays. The unique optical properties of titanium oxide have also led to its use in the production of pigments, such as white paint and coatings.[10]

Cerium oxide, also known as ceria, is an oxide of the rare earth metal cerium, denoted by the chemical formula CeO_2. Cerium can exist in either the free metal or oxide form, and can cycle between the cerous-cerium (III) and ceric-cerium (IV) oxidation states. Cerium oxide has a fluorite like cubic structure in which each cerium site is surrounded by 8 oxygen sites in Face centered cubic arrangement and each oxygen site has a tetrahedron cerium site.[11] It exhibits fascinating redox properties and is widely recognized for its catalytic and oxygen storage capabilities. Cerium oxide is commonly utilized as a catalyst in several industrial processes. Its redox property enables it to act as a catalyst in oxidation and reduction reactions, making it an essential component in automotive exhaust catalysts. The ability of cerium oxide to store and release oxygen contributes to efficient and cleaner combustion processes, ultimately reducing harmful emissions.[12] The unique optical properties of cerium oxide also make it a valuable component in optical lenses and glass coatings, providing anti-reflective properties and enhancing light transmission. Cerium and titanium mixed metal oxide, often referred to as CTMMO, is a composition of titanium dioxide (TiO_2) and cerium oxide (CeO_2). This combination results in a powerful material that exhibits remarkable functionality across a variety of applications.[13]

In this article, research was carried out to explore the potential of titanium oxide, cerium oxide, titanium and cerium mixed metal oxides. A work of fiction attempt has been made to synthesize and characterize titanium oxide, cerium oxide and a combination of titanium and cerium mixed metal oxides by microwave assisted co precipitation method.[14] The structural features, electrical, optical properties, topography of the metal oxides and mixed metal oxide nanoparticles were determined in depth with X-ray powder diffraction (XRD), field emission scanning electron microscope (FE-SEM), FT-IR spectroscopy, UV–visible absorption spectroscopy and atomic force microscopy. In recent years, there has been a growing interest in the development of gas sensors for various applications, including environmental monitoring, industrial processes, and health care.[15] Few materials that have shown great promise in gas sensing are titanium oxide and cerium oxide.[16] This has been extensively studied due to its distinct properties, which qualify it as an exceptional option for detecting different types of gases.[17]

MATERIALS AND METHODS:

The metal oxides and mixed metal oxides were synthesized using the microwave-assisted co-precipitation method. All chemicals utilized in this research were of analytical grade and were used without additional purification. The precursors, titanium oxychloride ($TiOCl_2$), and cerium chloride heptahydrate ($CeCl_3.7H_2O$), were purchased from Sigma Aldrich. The precipitant, sodium hydroxide (NaOH), was procured from HiMedia. All solutions were prepared by using double distilled water.

Preparation of metal oxide and mixed metal oxides nanomaterials :

Preparation of Titanium dioxide (TiO_2):

The synthesis of Titanium dioxide (TiO_2) nanoparticles was prepared by the following procedure. For this preparation, a 0.1M solution of titanium oxychloride ($TiOCl_2$) and a 0.3M solution of sodium hydroxide (NaOH) were prepared separately using double distilled water. Then, 0.3M NaOH was added dropwise to the 0.1M titanium oxychloride solution at a stirring rate of 500 rpm using a magnetic stirrer. Additionally, as the viscous of the mixture increased, the revolution of the magnetic Teflon was adjusted to maintain the stirring rate of 500 rpm throughout the experiment. The addition was continued until the required pH was achieved. After the addition was completed, stirring was continued for approximately 2 hours to

ensure overall good homogeneity. During stirring, a milky white suspension of $Ti(OH)_4$ was obtained from the aqueous clear solutions. The solution was then irradiated with microwaves using a household microwave oven for 15 minutes at 150 W. Then, the irradiated solution was sonicated for 30 minutes at a frequency of 52 kHz to improve the synthesized product's properties. The resulting precipitate was collected through filtration and washed with ethanol, followed by distilled water. It was then dried in a hot air oven at 110°C for 2 hours. This dried powder was subsequently annealed in a muffle furnace at 450°C for 3 hours to obtain pure white titanium dioxide.

Preparation of Cerium oxide (CeO_2):

In a classic synthesis, nanoparticles of cerium oxide (CeO_2) were prepared as follows. First, a solution of 0.1M cerium chloride heptahydrate was prepared using double distilled water. Additionally, a solution of 0.3M sodium hydroxide (NaOH) was also prepared separately. The 0.3M NaOH solution was then slowly added to the 0.1M cerium chloride solution while stirring at a rate of 500 rpm using a magnetic stirrer. Adjustments were made to the revolution of the magnetic teflon as needed to maintain the stirring rate throughout the experiment, especially when the viscous of the mixture increased. The addition continued until the desired pH was reached. Once the addition was complete, the stirring was continued for approximately 2 hours in order to achieve an overall good homogeneity. When cerium chloride heptahydrate reacts with sodium hydroxide, a hydrolysis process occurs and products such as cerium hydroxide are formed. Initially, the aqueous clear solution turns yellowish white, but as the reaction progresses, it converts into a light yellowish colloidal suspension. The solution is then subjected to microwave irradiation using a domestic microwave oven for 15 minutes at 150 W. Afterwards, the irradiated solution is sonicated for 30 minutes at a frequency of 52 kHz in order to obtain better properties of the resulting product. The resulting precipitate is collected through filtration, washed with ethanol followed by distilled water, and dried in a hot air oven at 110°C for 2 hours. The dried powder is subsequently annealed in the muffle furnace at 850°C for 2 hours. During calcination, the cerium hydroxide undergoes degradation and transforming into cerium oxide to acquire a pale yellowish colour.

Preparation of Cerium Titanium mixed metal oxide (CTMMO):

For the preparation of cerium–titanium mixed metal oxide, titanium oxychloride ($TiOCl_2$) and cerium chloride heptahydrate ($CeCl_3.7H_2O$) were used as precursors. Separate aqueous solutions of 0.1M $TiOCl_2$, 0.1M $CeCl_3$, and 0.3M sodium hydroxide (NaOH) were prepared using double distilled water. The aqueous solution of 0.3M NaOH was added drop by drop to the solution of 0.1M $TiOCl_2$ and thoroughly stirred using a magnetic stirrer. Then, 0.1M $CeCl_3$ solution was slowly added to this mixture and stirred well for about 2 hours using a magnetic stirrer. The solution was subsequently irradiated with microwaves in a domestic microwave oven for 15 minutes at 150 W. After that, the irradiated solution was sonicated for 30 minutes at a frequency of 52 kHz to achieve the product. The resulting precipitate was collected through filtration and washed with ethanol, followed by distilled water. It was then dried in a hot air oven at 110°C for 2 hours. The dried powder was subsequently calcined in a muffle furnace at 700°C for 2 hours to obtain the Cerium Titanium mixed metal oxide (CTMMO).

RESULTS AND DISCUSSION:

Characterization:

The FE-SEM images were captured using a JEOL JSM-6700F field emission scanning electron microscope. The XRD data was obtained using the PANalytical X'pert-pro powder X'celerator diffractometer with Cu-kα radiation. UV-visible absorption and fluorescence spectra were used by using quartz cells with a JASCO variant-630 spectrophotometer and a JASCO FP-6300 spectrofluorometer. KBR pellets were used to generate FT-IR spectra on a Shimadzu 8400S spectrometer in the range of 4000–400 cm^{-1}. The electrochemical investigations were conducted by CH-instrument Inc., based in TX, USA. The AFM images were obtained using a Nanosurf Easy Scan 2 controller. The measurements were conducted in contact mode, employing a micromachined Silicon probe.

In this research, two metal oxide nanoparticles, namely CeO_2 and TiO_2, as well as a Cerium Titanium mixed metal oxide, were synthesized. These nanoparticles were then characterized using various analytical techniques. The optical properties of the nanoparticles were investigated through UV-visible absorption (DRS) and FT-IR spectra. The crystal structure of the nanoparticles was examined using XRD analysis.

Microstructural analysis, including size, shape, and composition, was carried out using field emission scanning electron microscopy and energy dispersive X-ray (EDX) spectrometry. Atomic force microscopy was used to examine the topography images of the nanoparticles. The results obtained from these analyses are discussed below.

UV-Visible Absorbance Analysis (DRS):

The excitation of electrons to higher energy states can occur in atoms and molecules when they absorb UV-Visible light. This absorption of light leads to electronic excitation in each molecule.[18] The wavelength of the absorbed light corresponds to the unique chemical structure of the molecule. As a result, the absorption spectra can effectively aid in the qualitative identification of atomic and molecular species.

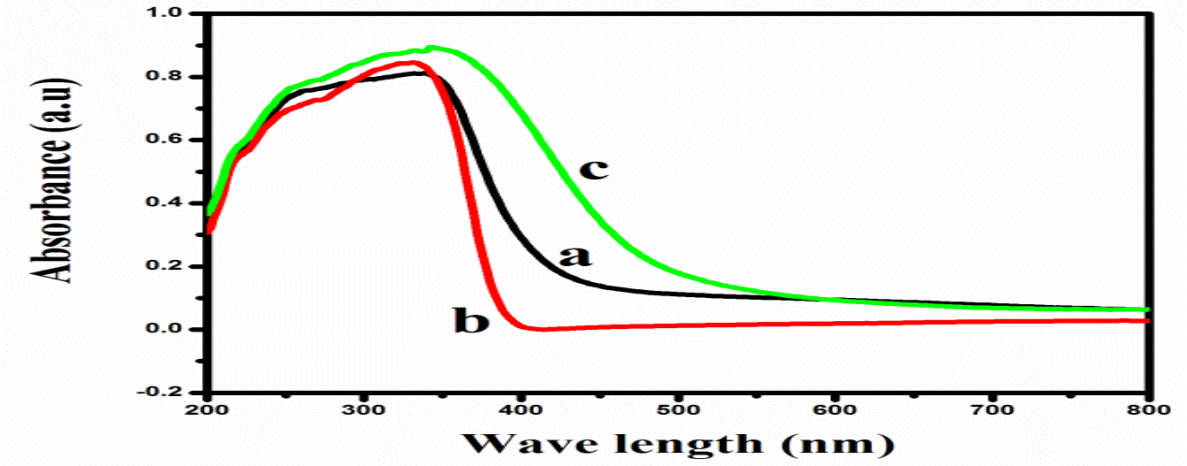

Figure.1. UV-Visible absorbance spectra of (a) CeO_2 (b) TiO_2 and (c) CTMMO

The UV-visible absorption spectroscopy technique was employed to investigate the optical properties of cerium oxide nanoparticles within the wavelength range of 200—900 nm. The obtained results of metal oxides are depicted in Fig. 1(a). A prominent absorbance peak was observed at a wavelength of 336 nm, with an absorbance value of 0.81 (<1), indicating a remarkable UV absorption capability of the synthesized cerium oxide nanoparticles.[19] It is worth noting that the absorbance level is influenced by various factors including band gap, oxygen deficiency, grain size, impurity centers, lattice strain, and surface roughness. The energy band gap of the material was determined utilizing the formula E = h. c /λ, where h represents Planck's constant, c represents the velocity of light, and λ represents the wavelength of maximum absorbance. The band gap energy of the CeO_2 nanoparticles was quantified using the aforementioned equation, and the band gap energy of CeO_2 is 3.69 eV. The titanium dioxide was exhibited an absorbance value (0.84) at a wavelength of 329 nm. This result signifies a favorable absorption capability within the UV region [20], and the band gap energy of the TiO_2 nanoparticles was measured and determined to be 3.77 eV. The study focused on analyzing the spectra revealed a prominent peak at a wavelength of 340 nm for the mixed metal oxide, which indicating a strong absorbance in the UV region, with an absorbance value of 0.88 signifying good absorbance. The band gap energy of the CTMMO nanoparticles was determined to be 3.65 eV. The band gap energy value for CTMMO is 3.65 eV which is lower than the CeO_2 (3.69 eV) as well as TiO_2 (3.77 eV). This means the semiconducting behavior of mixed metal oxides slightly increases when compared with the either CeO_2 or TiO_2.

Table.1. Absorption band (λ_{max}) and band gap energy values of CeO_2, TiO_2 and CTMMO.

S.No	Name of the samples	Absorption band (λ_{max}) (nm)	Band gap energy (eV)
1	Cerium oxide	336	3.69
2	Titanium oxide	329	3.77
3	CTMMO	340	3.65

Fourier Transform – Infra Red Spectral Analysis:

FT-IR spectroscopy serves as a valuable tool for identifying functional groups and examining the vibrational movement of atoms and molecules. This technique allows molecules to selectively absorb

specific frequencies of infrared (IR) light, which are determined by their unique characteristics.[21] The FT-IR spectra of CeO_2, TiO_2 and mixed oxides of Ce and Ti are given in Figure.2.

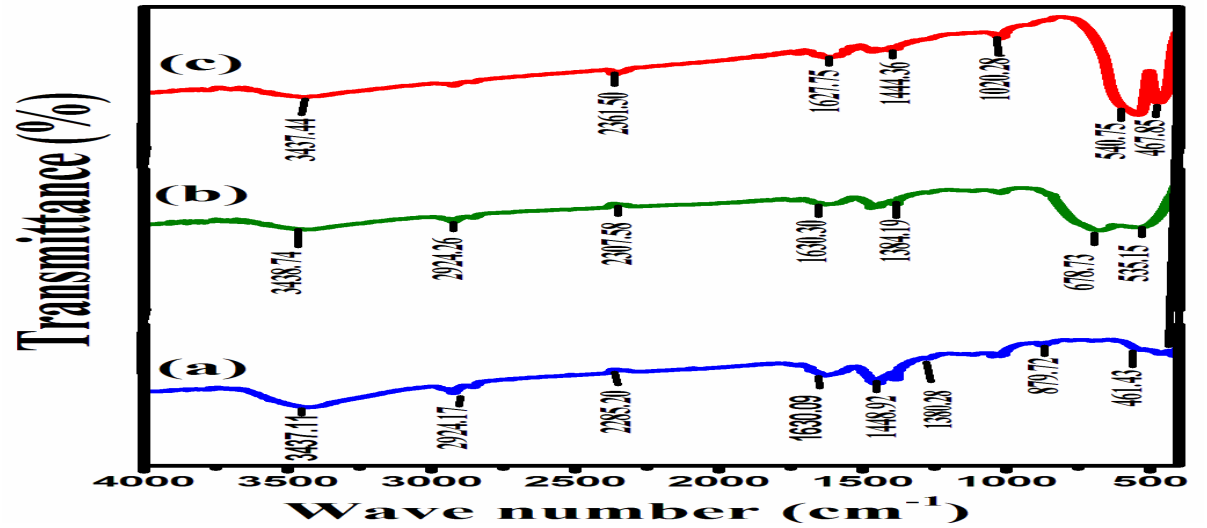

Figure.2. The FT-IR spectrum of (a) CeO_2 (b) TiO_2 and (c) CTMMO

The FT-IR spectra exhibited numerous significant absorption peaks within the 4000 cm^{-1} to 500 cm^{-1} range. The absorption peak spanning from 2200 cm^{-1} to 3450 cm^{-1} is attributed to the -OH stretching vibrations of H_2O. The peaks at 1380 cm^{-1} and 1630 cm^{-1} absorption bands corresponding to physically adsorbed water molecules. The FT-IR bands is appeared at 879.72 cm^{-1} and 461.43 cm^{-1}, which indicating the presence of CeO_2, which is characteristic of the Ce-O stretching vibrations [Fig.2(a)].[22] The FT-IR spectrum of TiO_2 is exhibited the absorption band observed at 3438.74 cm^{-1} signifies the stretching vibration of O-H, indicating the presence of H_2O [Fig.2(b)]. Similarly, the bending vibration of O-H can be attributed to the absorption band at 1630.30 cm^{-1}. The intense peak detected at 678.73 cm^{-1} corresponds to the characteristic Ti-O stretching band, specifically associated with TiO_2.[23] The FT-IR spectrum of CTMMO is displayed an absorption bands at 3437.44cm^{-1} and 1627.75 cm^{-1}, indicating the presence of titanium. Additionally, the absorption bands at 1444.36 cm^{-1} and 467.85 cm^{-1} were observed, signifying the existence of cerium. Overall, this implies that the formation of a cerium titanium mixed metal oxide [Figure.2(c)].

Table.2. Shows the assigned functional groups of 1) CeO_2, 2) TiO_2 and 3) CTMMO

S.No	Assigned functional groups	Name of the samples		
		CeO_2 (cm^{-1})	TiO_2 (cm^{-1})	CTMMO (cm^{-1})
1	O-H Stretching vibration	2285.20 3437.11	2307.58 3438.74	2361.50 3437.44
2	O-H bending vibration	1380.28 1448.92 1630.09	1384.19 1630.30	1444.36 1627.75
3	M-O stretching vibration	461.43 879.72	535.15 678.73	467.85 540.75

X-ray Diffraction Analysis:

The crystallinity of the synthesized CeO_2 sample was assessed using X-ray diffraction analysis.[24] The X-ray diffraction pattern of the CeO_2 particles was displayed in the Figure 3(a). The structural identification of the cerium oxide nanoparticles was conducted by analyzing the X-ray diffraction within the 2θ range of 20° to 80°. The diffraction pattern was exhibited distinct peaks corresponding to (111), (200), (220), (311), (222), (400), (331), and (422) planes, which indicated that the CeO_2 has exhibited the face-centered cubic fluorite structure. These peaks matched perfectly with the pure cubic fluorite structure of CeO_2, with a lattice constant of a=5.411 Å, aligning with the JCPDS file No. 75-0076.[22] The particle size of the cerium

oxide nanoparticles was estimated using Scherrer's equation: $D_{hkl} = 0.899 \lambda / \beta \cos \theta$, where λ represents the X-ray wavelength, θ is the Bragg diffraction angle, and β corresponds to the full width half maximum (FWHM) of the XRD peak observed at the diffraction angle θ.[25-26] This calculation is yielded the average crystalline size of CeO_2 and it was approximately 7.06 nm.

The titanium oxide samples displayed characteristic peaks relating to (110), (101), (111), (210), (211), (220), (002), and (310) planes in figure 3(b). These observations matched the tetragonal structure, as stated in JCPDS file No. 89-4920 [27], further confirming the findings. The average size of the crystalline structures was determined using the Scherrer equation based on the X-ray line broadening analysis, yielding a value of approximately 5.75 nm. Similarly the diffraction peaks of mixed oxides was observed at angles 2θ=25.47°, 37.91°, 48.15°, 53.99°, 55.16°, 62.78°and 75.12° are clear indicated that the presence of certain crystallographic planes (109), (101), (220), (210), (211), (002) and (331) in TCMMO [figure.3(c)]. As a result, the calculated average crystalline size was approximately 5.83 nm. The reduction in crystal size can be attributed to the incorporation of Ti–O–Ce within the mixed metal oxide of CTMMO lattice. The crystallite size of oxides are tabulated in the Table 3.

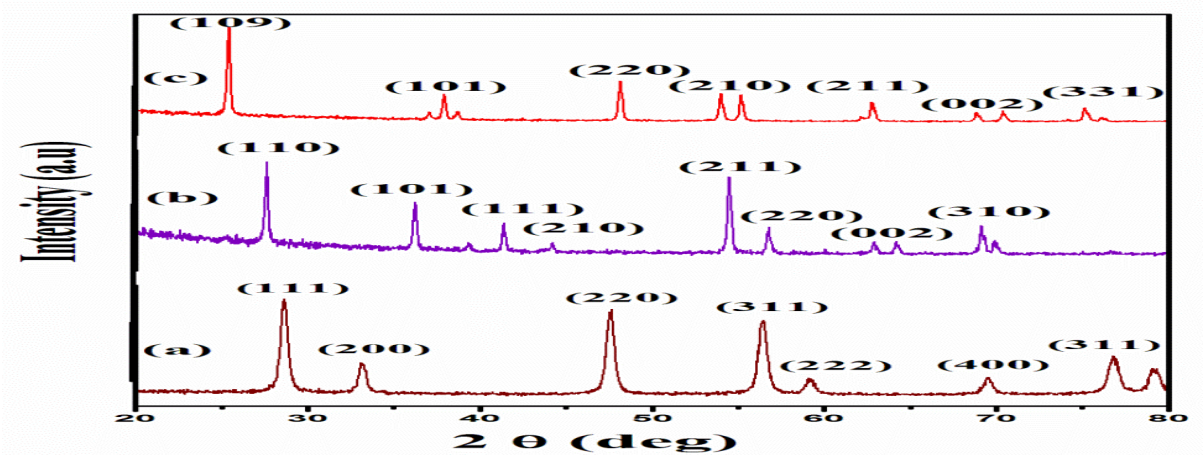

Figure.3. X-Ray Diffraction pattern of (a) Cerium oxide (b) Titanium oxide and (c) CTMMO

Table.3 Crystallite size of 1) Cerium oxide, 2) Titanium oxide and 3) CTMMO

S.No	Name of the samples	Crystallite size (nm)
1	CeO_2	7.06
2	TiO_2	5.75
3	CTMMO	5.83

Energy-Dispersive X-Ray Analysis (EDAX):

The determination of the elemental composition of metal oxides and mixed metal oxides was conducted using Energy Dispersive X-ray Spectroscopy (EDS).[28] This analytical technique involves the recording of characteristic X-rays by an energy dispersive spectrometer, enabling the identification of elements present as well as assessing their respective concentrations. The EDAX spectra of nanomaterials are given in the Figure 4.

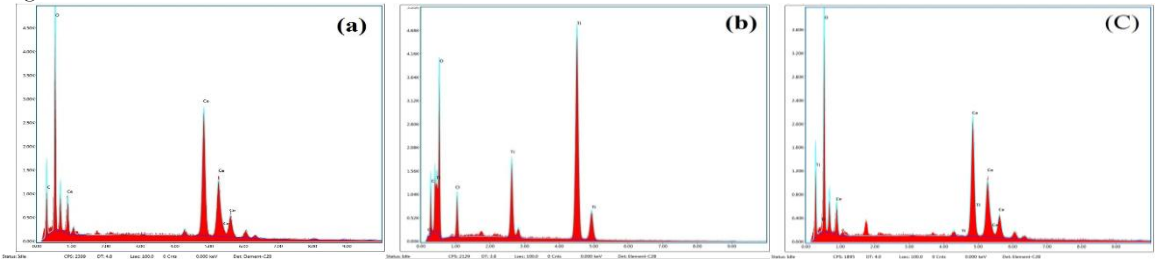

Figure.4. EDAX Spectral images of (a) Cerium oxide (b) Titanium oxide (c) CTMMO

The analysis of CeO_2 using Energy Dispersive Spectroscopy (EDS) is presented in Figure 4 (a), confirming the presence of both Ce and O elements in terms of their weight percentages. The EDS, is employed in conjunction with Scanning Electron Microscopy (SEM), enabled the examination of the chemical

composition of the material.[29] The obtained EDS spectrum clearly exhibits peaks corresponding to cerium and oxygen, indicating their existence within the sample. The weight concentration of cerium and oxygen, accounting for a total of 96.86%, further ensures the high purity of the cerium oxide nanoparticles. The energy dispersive spectroscopy (EDS) analysis of TiO_2 confirming the presence of titanium (Ti) and oxygen (O) in the material, as evidenced by their respective weight percentages. The peaks observed in the EDS spectrum indicate the presence of titanium and oxygen. Furthermore, the analysis of the EDS spectrum revealed that the titanium oxide nanoparticles obtained are of high purity, with the combined weight concentration of titanium and oxygen accounting for 94.47% of the total composition. The Energy Dispersive Spectroscopy (EDS) analysis of CTMMO, which firmly verifies the presence of cerium, titanium, and oxygen in both weight percent and atomic percent. The EDS analysis reveals distinct peaks corresponding to the elements cerium, titanium, and oxygen. The obtained EDS spectrum unequivocally demonstrates the presence of cerium, titanium, and oxygen, thereby confirming the near-purity of the cerium titanium mixed metal oxide nanoparticles. This confirmation is further bolstered by the weight concentration of cerium, titanium, and oxygen, which collectively amounts to 100.00%.

Table.4. Elemental composition of (a) Cerium oxide (b) Titanium oxide and (c) CTMMO

a) Cerium oxide			**b) Titanium oxide**			**c) CTMMO**		
Element	**Weight %**	**Atomic %**	**Element**	**Weight %**	**Atomic %**	**Element**	**Weight %**	**Atomic %**
C K	3.14	20.48	**C K**	5.53	13.3	**O K**	21.7	72.7
O K	16.45	49.40	**O K**	47.24	62.63	**Ti K**	35.16	12.25
Ce L	80.41	30.12	**Ti K**	47.23	24.07	**Ce L**	43.14	15.05
Total	100	100	**Total**	100	100	**Total**	100	100

Field Emission Scanning Electron Microscope analysis:

The investigation into the morphology and structure of the samples was carried out utilizing Field Emission Scanning Electron Microscopy (FE-SEM).[30] The FE-SEM images of CeO_2, TiO_2 and mixed oxides are exhibited in the Figure 5. The surface analysis of prepared CeO_2 was involved in the measurement of SEM micrographs and subsequent topographical analysis.[31] The FE-SEM images (Figure.5) reveals that the prepared nanomaterials were uniform in size, shape and not agglomerated. The results revealed that the synthesized CeO_2 nanoparticles exhibited a uniformly spherical shape with a smooth and homogeneous structure. The average particle size estimated from FE-SEM images is about 18 nm (figure.5a).[32] The surface of TiO_2 metal oxide was examined, and a topographical analysis was conducted. The synthesized TiO_2 nanoparticles exhibited a smooth, spherical shape.

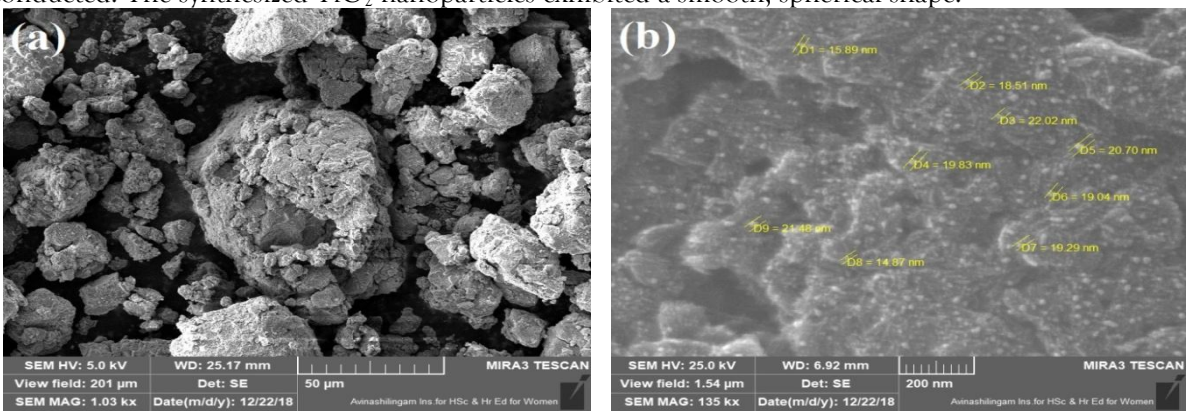

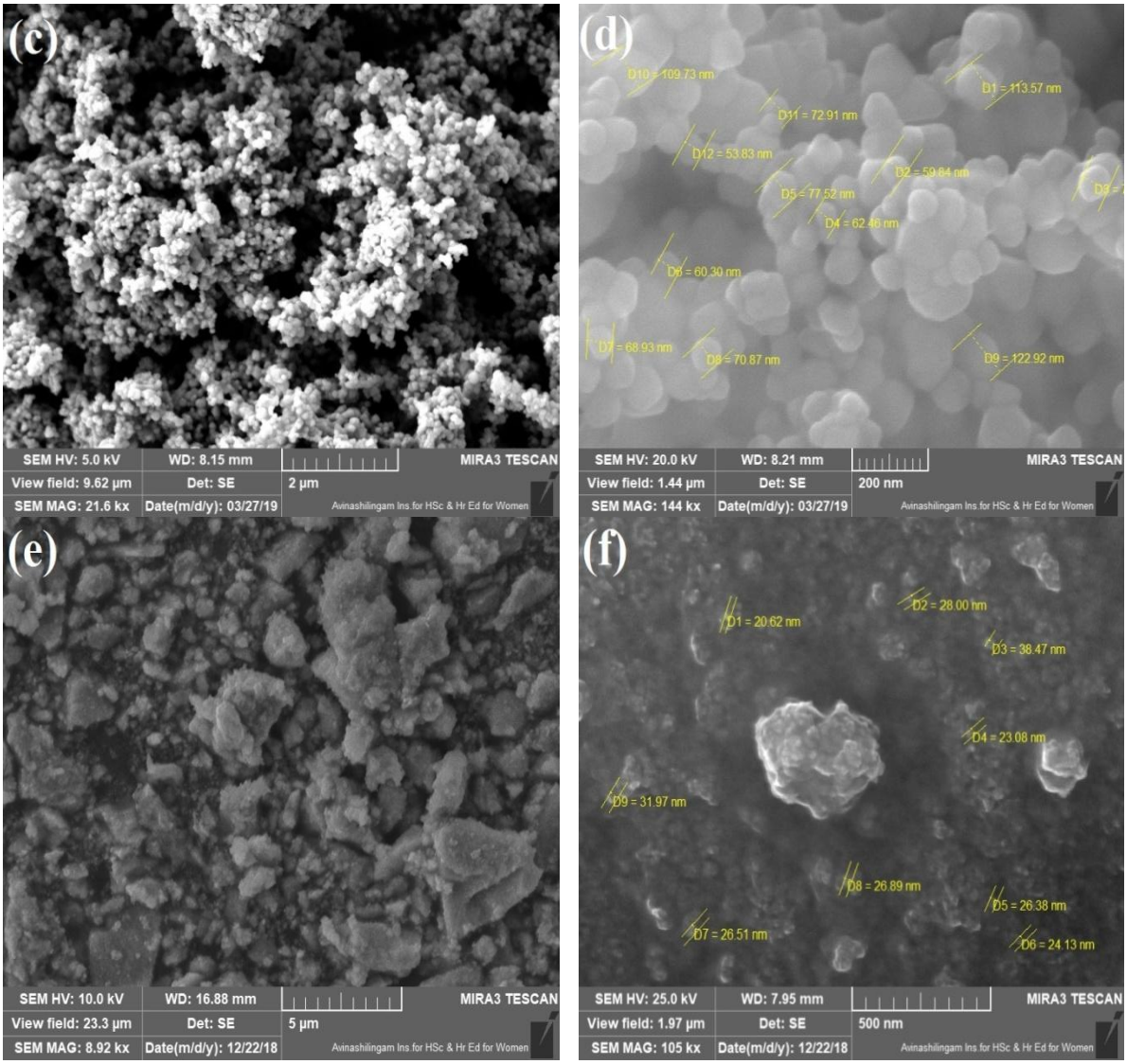

Figure.5. FESEM images of (a-b) Cerium oxide, (c-d) Titanium oxide, (e-f) CTMMO

Additionally, microscopic images revealed a uniform distribution of particles with a homogeneous structure, free from any abnormal formations on the surface in Figure.5 (c). These images, captured at different magnifications, provided a clear understanding of the physical morphology, particle size, and aspect ratio of the synthesized nanoparticles. The CTMMO, which had been prepared, displayed a cluster-like structure under a magnification of 500 nm having average particle size of 26 nm (figure.5f). It is evident from the figure.5 that the prepared nanomaterials were smaller in size having uniform shape and equal particle size distribution.

Atomic Force Microscope:

The morphology of the prepared nanomaterials were carried by using atomic force microscope. All scans were conducted under ambient conditions, known to yield satisfactory topography outcomes.[33] The images were recorded in topography mode with a resolution of 256x256 pixels and a scan rate ranging from 0.5 to 1 Hz. For height measurements of adsorbed NPs and agglomerates, the microscope's section analysis software was employed. The AFM images of CeO_2, TiO_2 and mixed oxides of Ce and Ti are given in the figure.6. The image reveals that the prepared nanomaterials has well separated conical nano columnar structure. To characterize the surface topography, the roughness parameters are very essential. Table 5 lists the most common parameters of area roughness. The average roughness (S_a) and the root mean square roughness (S_q) are evaluated over the complete 3D surface respectively. Particularly, root mean square roughness (S_q) is used to study the temporal changes in the creation of a new surface as well as spatial differences when studying the surface feature using different scales.

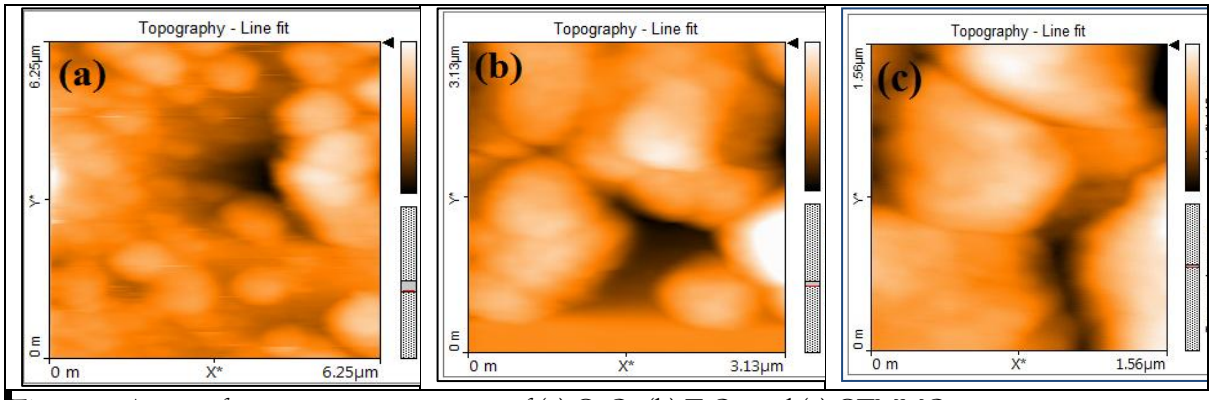

Figure.6. Atomic force microscope images of (a) CeO_2 (b) TiO_2 and (c) CTMMO

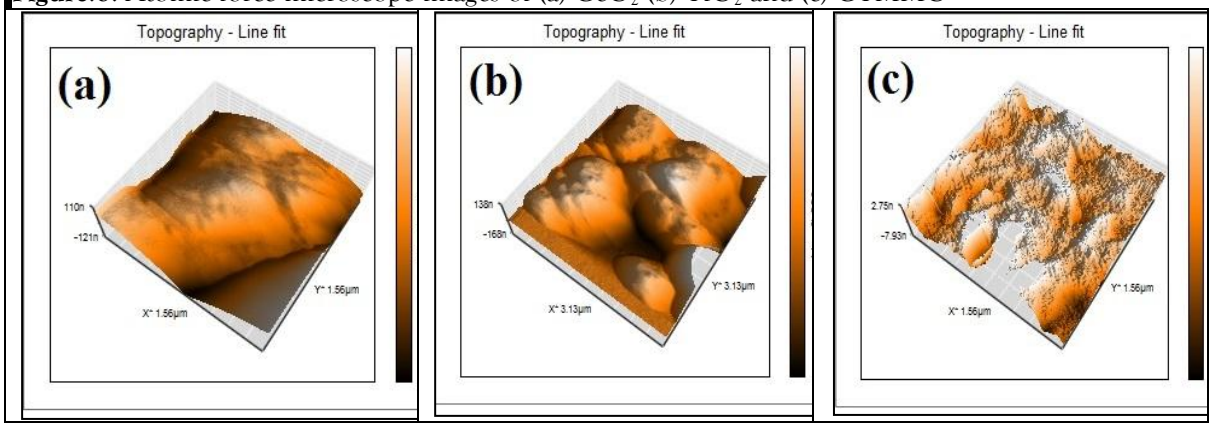

Figure.7. Atomic force microscope 3D view of (a) CeO_2 (b) TiO_2 and (c) CTMMO

The Atomic Force Microscope (AFM) allows for 3D characterization of nanoparticles with nanometer resolution shown in figure.7. In figure.7 (c), the contact mode AFM image showcases the samples that underwent annealing at a temperature of 700°C. The image distinctly features spherical structures that are nicely separated. Notably, this image has been analyzed for area roughness, for CTMMO. The below tabulated values indicates that the presence of a substantial surface area in the synthesized nanomaterials.

Table.5. Area roughness of CeO_2, TiO_2 and CTMMO from AFM spectroscopy

Area Roughness			
Area Parameter	**CeO_2**	**TiO_2**	**CTMMO**
Area	39.37 pm^2	39.84 pm^2	39.37 pm^2
S_a	54.07 nm	42.27 nm	7.36 nm
S_q	71.39 nm	57.15 nm	10.52 nm
S_y	498.70 nm	409.13 nm	108.09 nm
S_p	249.74 nm	244.06 nm	75.15 nm
S_v	-248.93 nm	-165.18 nm	-32.98 nm
S_m	-35.91 fm	-37.25 fm	-18.62 fm

Sensing analysis of CeO_2, TiO_2 and mixed oxides of CTMMO:

Electrochemical Studies:

The general mechanism involves the target analyte coming in contact with the sensing material and reacting with pre-adsorbed surface molecules (usually oxygen), promoting electron exchange and resulting in a measurable change in conductivity.[34] The goal in this study was to assess the ability of the sensors to detect ammonia and H_2S gas.[35] In this research work, the voltammetric studies were carried out at pH-7.00 buffer solution using glassy carbon electrode. A CH-instrument Inc., was used for the CV measurements using a three electrode cell containing glassy carbon electrode as working electrode, platinum wire as counter electrode and a saturated calomel electrode (SCE) as reference electrode.[36] Potential cycling between +0.4 V to -1.6 V was carried out in pH-7.00 buffer solution at a scan rate of 20 mV/s. Ammonia and Hydrogen sulphide is a highly toxic gas that is commonly found in many industrial

and agricultural environments.[37] It is essential to detect and monitor ammonia levels to ensure the safety and well-being of workers and the surrounding environment. The metal oxide-based gas sensors have shown remarkable sensitivity and selectivity towards ammonia detection.[38] One of the key mechanisms behind the gas sensing properties of metal oxide is its ability to adsorb and react with gas molecules.[39] When exposed to ammonia, metal oxide undergoes a surface reaction, resulting in a change in its electrical conductivity. By measuring the change in conductivity, the presence and concentration of ammonia and hydrogen sulphide can be accurately determined.

Recognition of ammonia (NH_3):

The prepared nanomaterials were subjected to cyclic voltammogramms scanning ranging from -1.4 V to 0.4 V. Throughout the cyclic voltammograms, no evident response was detected on the bare glassy carbon electrode which was named as (I). However, a reduction peak was observed for the modified GCE with metal oxides such as cerium oxide, titanium oxide and CTMMO due to their oxygen storage capacity which was designated as (II). The addition of 1mM of ammonia solution to the system resulted in a peak current shift and transformation of the broad peak into a distinct and narrow peak indicating an increasing peak current value due to the adsorption of ammonia on the surface of the electrode. This change clearly demonstrated the sensing capability of CeO_2, TiO_2, and CTMMO towards ammonia, referred to as (III). conversely, on the mixed metal oxide, the oxidation peak current at E=0.110V, i=3.013e^{-6}A for ammonia shown in figure.(c) were evident, showing a clear and sharp profile indicating an increased adsorption of ammonia upon the incorporation of metal oxides. When comparing CTMMO to the peak current values of cerium oxide and titanium oxide, it exhibits higher peak current values. This confirms the good sensing capability of CTMMO towards ammonia. The overall potential scan rate for the cyclic voltammograms was 20 mV/s.

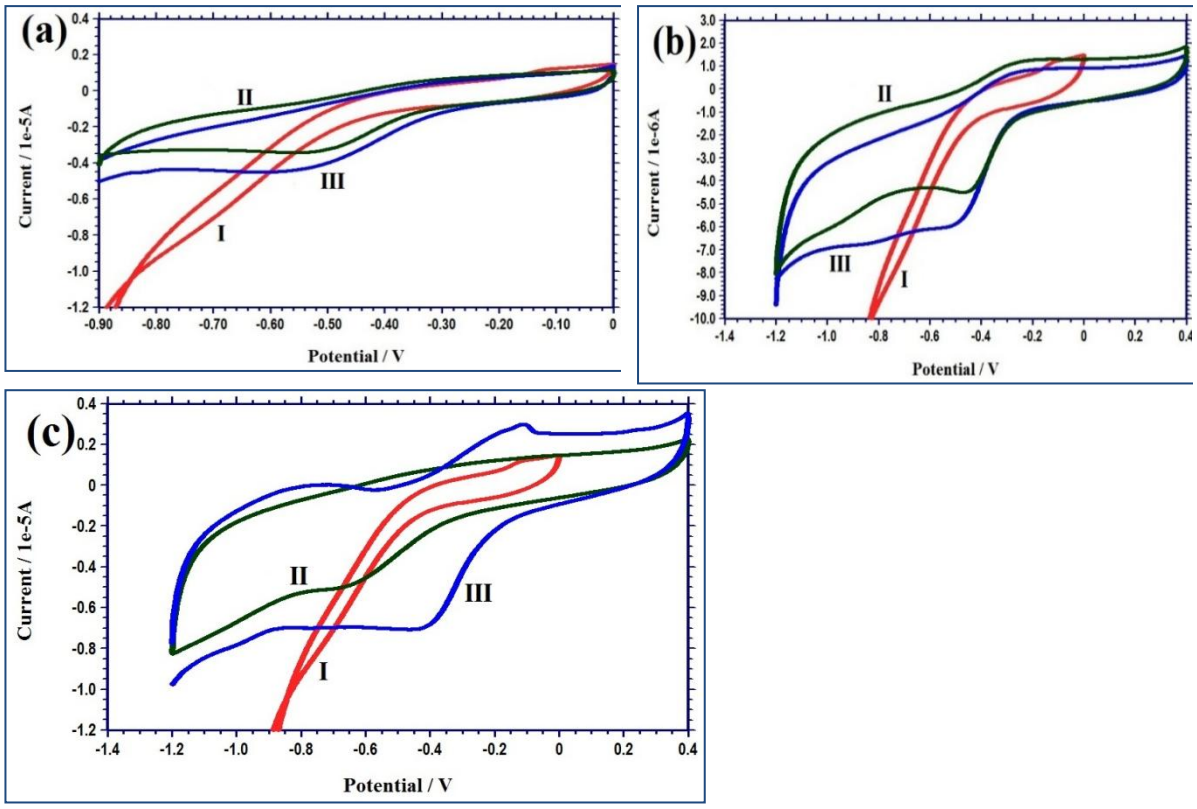

Figure.8. Cyclic Voltammogram of ammonia on (a) Cerium Oxide, (b) Titanium Oxide and (c) CTMMO

Table 6. Cyclic voltammogram behavior of ammonia.
[Ph=7.00, scan rate=20 mV/s]

S.No	Types of Electrode	Peak current of Modified GCE		Peak current of Modified GCE + Addition of Ammonia	
		$-E_{pc}$ (mV)	$-i_{pc}$ (µA)	$-E_{pc}$ (mV)	$-i_{pc}$ (µA)
A	CeO_2 Modified GCE	0.519	3.370	0.582	4.469
B	TiO_2 Modified GCE	0.460	4.533	0.503	5.973
C	CTMMO Modified GCE	0.649	4.819	0.413	6.981

Recognition of Hydrogen Sulphide (H_2S):

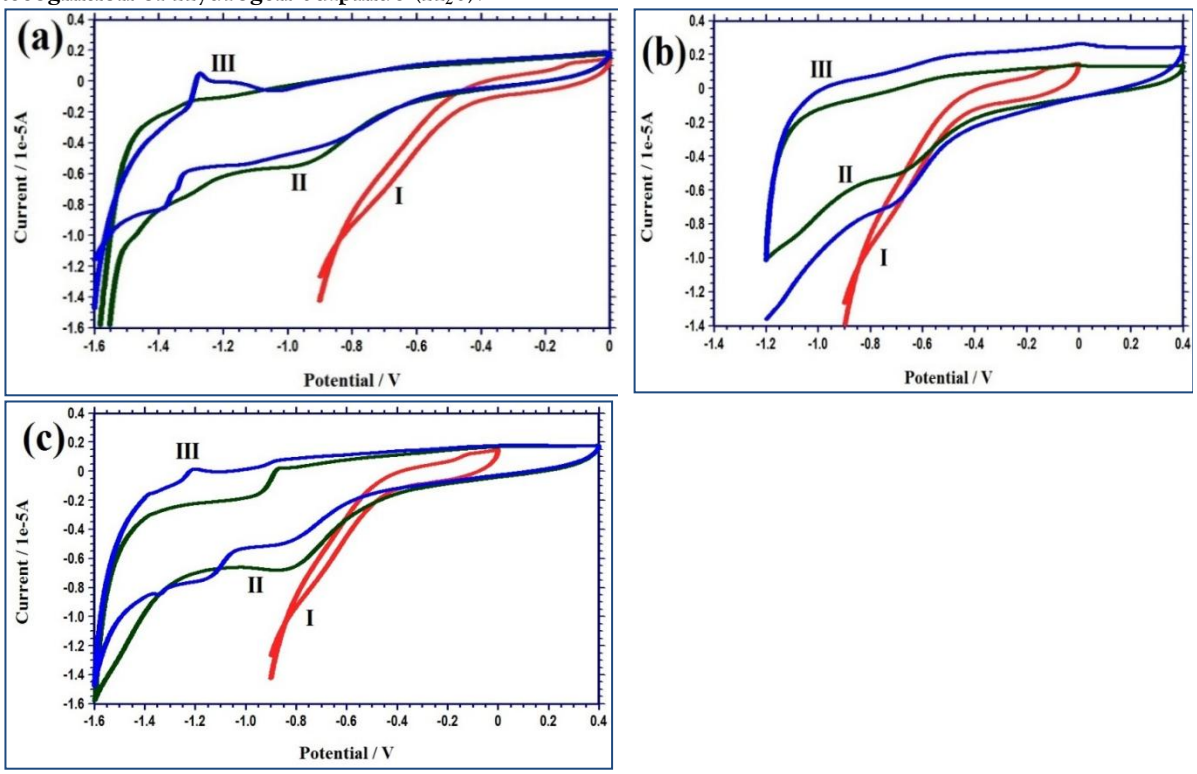

Figure.9. Cyclic Voltammogram of H_2S on (a) Cerium oxide, (b) Titanium oxide and (c) CTMMO

Cyclic voltammograms of prepared nanomaterials was scanned from -1.6 V to 0.4 V. The potential scan rate for the cyclic voltammograms was 20 mV/s. In the overall cyclic voltammograms, no peak response was observed for a bare glassy carbon electrode which was designated as (I). A lower response in peak current was observed when the GCE was modified with metal oxides like cerium oxide, titanium oxide, and CTMMO which was denoted as (II). After the introduction of 1mM of H_2S solution to the cell, the observed peak current exhibited a noticeable shift and shows a increase in peak current value due to the adsorption of H_2S on the surface of the electrode. This increase in peak current signifies the successful sensing ability of CeO_2, TiO_2, and CTMMO towards H_2S, denoted as (III). Moreover, for ceria, the oxidation peak current occurred at E=1.270V and i=4.453e^{-7}A and for the mixed metal oxide of CTMMO, the oxidation peak current was observed at E=1.205V and i=9.6008e^{-7}A, revealing an higher adsorption of H_2S. It is further evident that the higher peak current values of CTMMO confirm its better sensing ability towards H_2S.

Table 7. Cyclic voltammogram behavior of H_2S.
[Ph=7.00, scan rate=20 mV/s]

S.No	Types of Electrode	Peak current of Modified GCE		Peak current of Modified GCE + Addition of H_2S	
		$-E_{pc}$ (mV)	$-i_{pc}$ (μA)	$-E_{pc}$ (mV)	$-i_{pc}$ (μA)
a	CeO_2 Modified GCE	0.940	5.270	1.274	5.401
b	TiO_2 Modified GCE	0.680	4.880	0.702	6.846
c	CTMMO Modified GCE	0.834	6.704	1.154	7.450

Binding Interaction of Nanomaterials with the Biomolecule Ovalbumin:
The significance of comprehending the binding interactions among molecules in protein research cannot be overstated. An intriguing area of study in this domain involves exploring ovalbumin binding interactions through UV-visible absorption spectral titrations.[40] This approach allows for a deep dive into the complex dynamics of these interactions, shedding light on various aspects of protein behavior and function.

UV-Visible absorption spectral responses of Ovalbumin:
The UV-Visible absorption spectral titrations involved the gradual addition of a metal oxide into a protein solution while monitoring changes in the absorbance spectrum. This technique provides valuable information about the binding affinity, stoichiometry, and thermodynamics of the interaction. The binding interaction between proteins and nanoparticles usually involves looking at the changes in the absorbance spectra at 209 nm, and the binding constant (Kα) value is calculated from the absorption spectral changes. The spectral titration of nanoparticles and ovalbumin was undertaken by keeping the concentration of ovalbumin (20 μM) is constant and varying the concentration of nanoparticles from 0 to 30 μM. The absorption intensity of ovalbumin at 209 nm decreases with increasing the concentration of nanoparticles. The UV-visible absorption spectra of ovalbumin with the addition of nanoparticles are shown in fig. 10. The binding constant (Kα) values are calculated using the equation and are displayed in Table (8).

Fluorescence spectral responses of Ovalbumin:
Fluorescence spectral titrations quenching, also known as fluorescence quenching, is a widely used technique in molecular spectroscopy for investigating the interactions between fluorescent molecules and quenchers. This method assesses the decrease in fluorescence intensity of a fluorescent analyte caused by the presence of a quencher. The quencher can be a small molecule, a metal ion, or a biomolecule. Fluorescence quenching occurs due to various molecular interactions, such as energy transfer, molecular rearrangements, the formation of ground state complexes, excited state reactions, and collisional diffusion. These interactions can induce quenching through dynamic quenching or state quenching techniques. Dynamic quenching takes place when an excited state fluorophore collides with a quencher molecule in a solution, causing a decrease in fluorescence intensity. Through diffusion, during an interaction with the quencher, the fluorophore returns to its ground state, forming a ground state complex with the quencher and resulting in static quenching.

The fluorescence emission spectrum of ovalbumin shows an emission peak at 331 nm when it was excited at 280 nm. When various concentrations of prepared nanoparticles from 0 to 30 μM are added to a fixed concentration of ovalbumin (20μM), the fluorescence intensity decreases as the nanoparticle concentration increases. This decrease in intensity is due to the interaction between the nanoparticles and ovalbumin, as shown in Figure.11. The Stern-Volmer plot was created and shown in figure.12 using the emission spectral data and the values for the Stern-Volmer constant (Ksv) and bimolecular quenching constant (Kq) were calculated and recorded in Table 8.

International Journal of Environmental Sciences
ISSN: 2229-7359
Vol. 11 No. 18s, 2025
https://theaspd.com/index.php

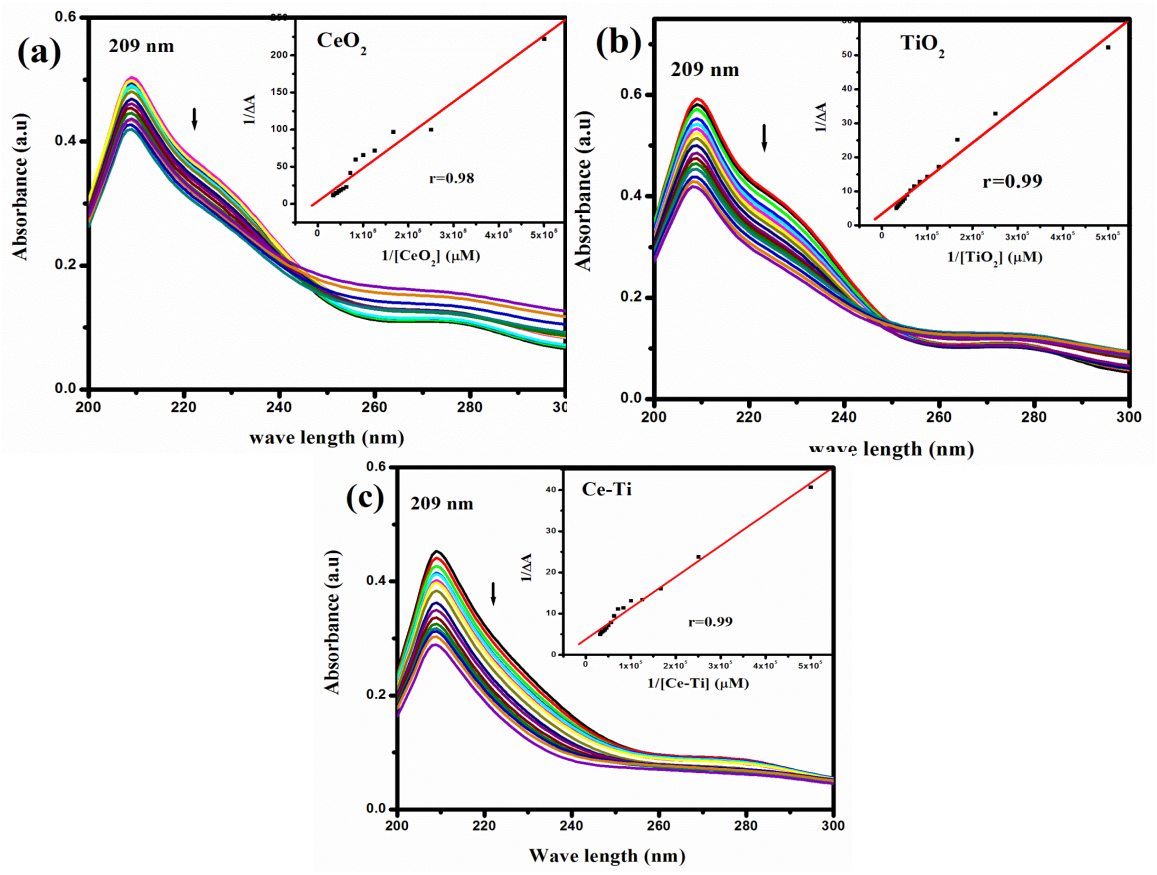

Figure.10. UV-visible absorption spectra of ovalbumin (20 μM) upon gradual addition of various concentrations (0 to 30 μM) of (a) CeO_2, (b) TiO_2 and (c) CTMMO (Ce-Ti) Inset **:** linear double reciprocal plot.

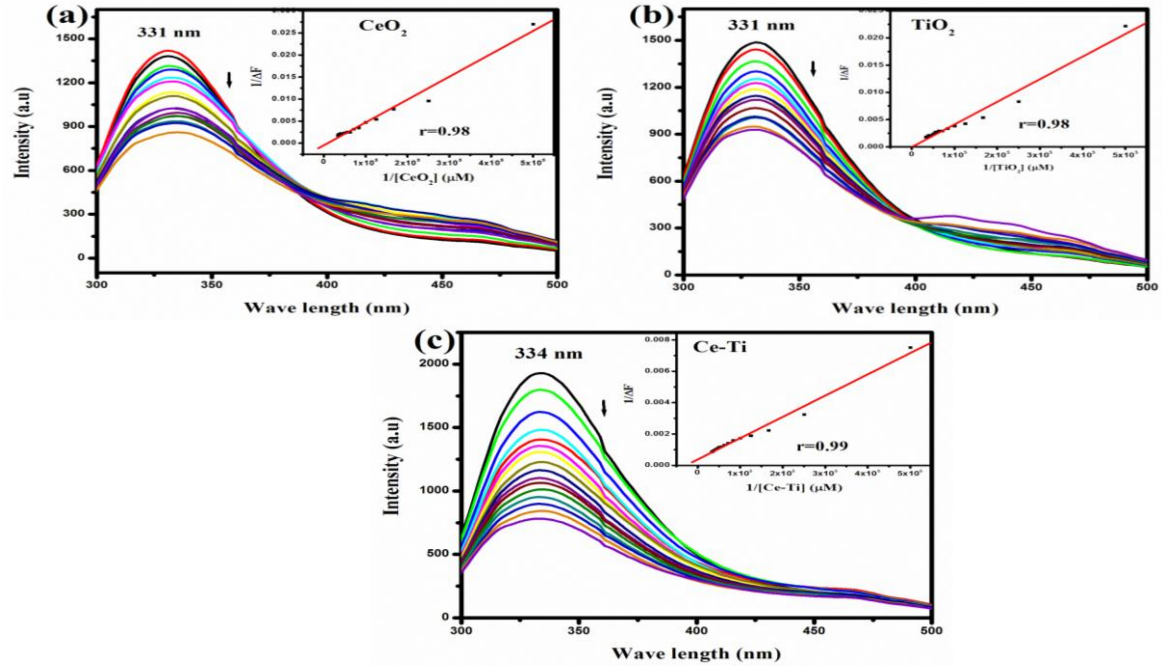

Figure.11. Fluorescence emission spectra of Ovalbumin (20 μM) upon gradual addition of various concentrations (0-30 μM) of (a) CeO_2, (b) TiO_2 and (c) CTMMO (Ce-Ti) Inset **:** Modified Benesi-Hildebrand plot.

The interaction between the nanoparticles CeO_2, TiO_2, and CTMMO (Ce-Ti) (as shown in the Figures) has been analyzed to determine the binding parameters. The results indicate that the metal oxide

nanoparticles prepared in this study can significantly suppress the intrinsic fluorescence of ovalbumin. Moreover, the obtained quenching rate constant (kq) exceeds the widely accepted maximum diffusion constant of biomolecules, which is 2.90 x $10^{10}M^{-1}S^{-1}$.[41] These findings suggest that the binding between ovalbumin and metal oxide nanoparticles follows the static quenching mechanism.

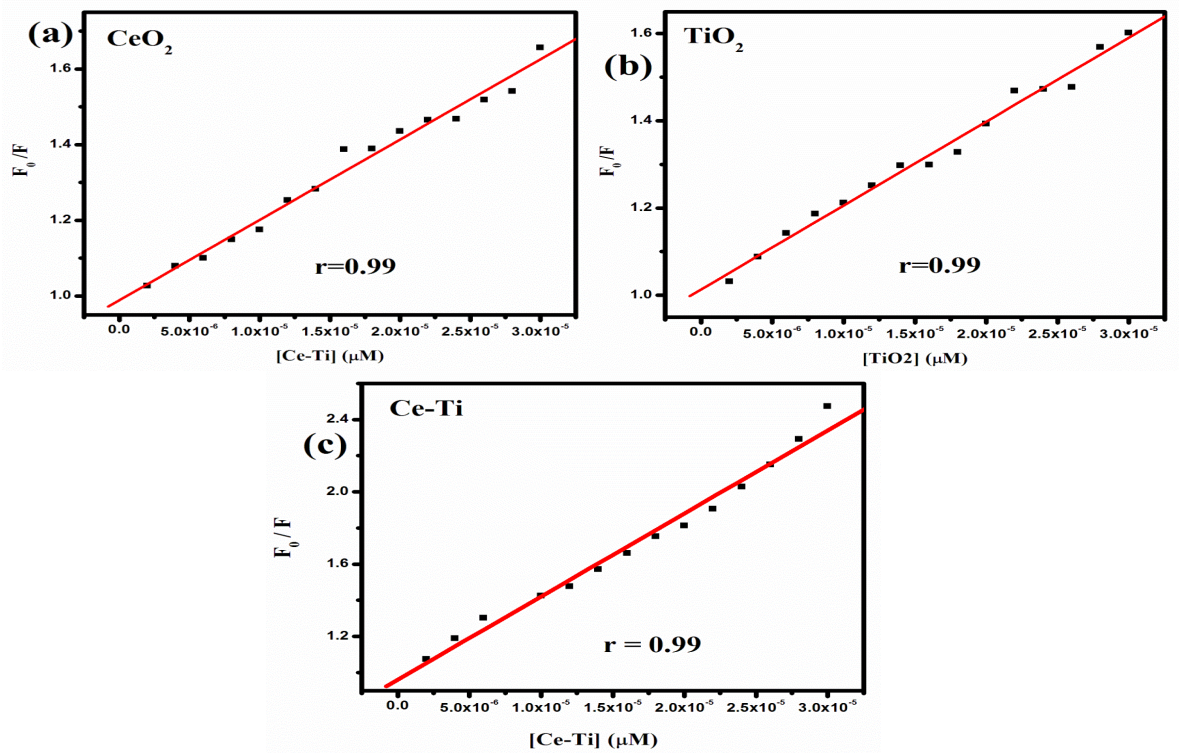

Figure.12. Stern-Volmer plot of (a) CeO_2, (b) TiO_2 and (c) CTMMO (Ce-Ti)

Table.8. Binding parameters of nanomaterials with Ovalbumin from spectral data.

S.No	Name of the samples	Absorption (UV)		Emission (Flouresence)					
		λmax (nm)	Ka (M^{-1})	λem (nm)	K_{sv} (M^{-1})	k_q($M^{-1}s^{-1}$)	K_b(M^{-1})	K_{app}(M^{-1})	n
1	CeO_2	209	$4.31x10^4$	331	$4.65x10^5$	$4.65x10^{13}$	$5.330x10^4$	$8.62x10^4$	1.13
2	TiO_2	209	$3.24x10^4$	331	$5.26x10^5$	$5.26x10^{13}$	$6.309x10^3$	$2.18x10^4$	1.00
3	CTMMO	209	$1.15x10^5$	335	$2.12x10^5$	$2.12x10^{13}$	$6.546x10^3$	$5.12x10^4$	1.01

Antibacterial activities of synthesized nanomaterials:

In this article, research work was delved into the fascinating world of metal oxides and their remarkable ability to combat bacteria and other pathogens, highlighting their effectiveness.[42] Metal oxides, formed through the reaction of metals with oxygen, have long been utilized for their diverse range of properties. While their applications span various industries, it is their anti-bacterial activity that has garnered significant attention in recent years. These compounds have emerged as compelling alternatives to traditional antibiotics, offering a promising solution to combat the rise of antibiotic resistance.[43]

Antibacterial activity of CeO_2, TiO_2 and CTMMO:

The antibacterial activity of metal oxide nanoparticles has received marked global attention as they can be specifically synthesized to exhibit significant toxicity to bacteria. The antibacterial activity of

nanomaterials can be carried by disc diffusion method. The test bacteria were inoculated in peptone water and incubated for 3 – 4 hours at 35°C. Mueller Hinton agar plates were prepared and poured into sterile petri plates. 0.1 ml of bacterial culture was inoculated on the surface of Mueller Hinton agar plates and spread using an L-rod. The inoculated plates were allowed to dry for five minutes. The disk loaded with a sample concentration of 1000 µg/ml was placed on the surface of the inoculated petri plates using sterile technique. The plate was incubated at 37°C for 18-24 hours. The plate was examined for an inhibitory zone, and the zone of inhibition was measured in mm. Invariably all the three nanoparticles showed good antibacterial activity; inhibit the growth of pathogen considerably. The maximum level of zone of inhibition (15 mm) was observed for CTMMO (Ce-Ti) against Pseudomonas aeruginosa. Thus from the zone of inhibition; it was evident that the synthesized metal oxide nanoparticles have potent antibacterial activity. The Antibacterial activity of Zone of inhibition levels are shown in Table: (9).

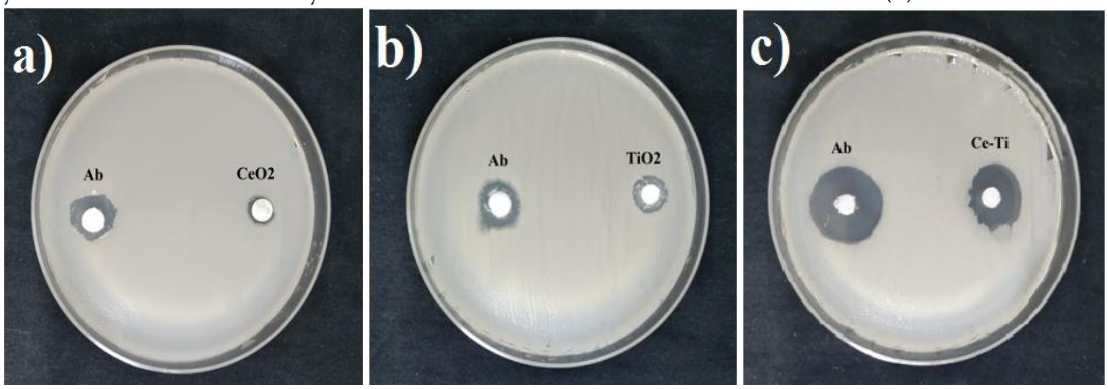

Figure.13. Antibacterial activity of (a) CeO_2 (b) TiO_2 (c) CTMMO for E.coli bacteria

Table.9. Antibacterial activity Zone of inhibition levels for CeO_2 , TiO_2 and CTMMO

Bacteria	Inhibition zone in mm					
	Ab Ampicillin	CeO_2	Ab Ampicillin	TiO_2	Ab Ampicillin	CTMMO
E.coli	12	7	9	8	17	12
Staphylococcus aureus	8	6	12	9	16	11
Bacillus subtilis	10	8	14	9	19	15
Bacillus cereus	7	8	9	6	13	8
Pseudomonas aeruginosa	9	7	9	8	17	15

CONCLUSION:

Cerium oxide, titanium oxide, and mixed metal oxides of CTMMO were synthesized using the microwave-assisted co-precipitation method. The synthesized nanoparticles were characterized using FT-IR, UV-VIS (DRS), XRD, FE-SEM, AFM, and EDAX. The surface morphology of the metal oxide nanoparticles was characterized using FE-SEM, revealing different morphological structures. XRD results confirmed that the synthesized product consisted of nanocrystallites. The XRD pattern also confirmed the cubic fluorite structure of CeO_2. EDAX results revealed the composition of the samples, confirming their high purity. The electrochemical studies of cyclic voltammetry shows clear and sharp oxidation peaks for ammonia on mixed metal oxides of CTMMO and for Hydrogen sulfide on cerium oxide and mixed metal oxide of CTMMO, indicating an enhanced sensing performance. From this study Titanium oxide-based gas sensors offer a promising solution for sensing ammonia and hydrogen sulfide due to their sensitivity, selectivity and stability. The development of these sensors opens up new possibilities for applications in industrial, environmental, and medical fields. The prepared nanoparticles were quenched by Ovalbumin by using the static quenching process. The prepared compounds showed good antimicrobial activity against the following bacteria E.coli, Bacillus subtilis, Bacillus cereus, Pseudomonas aeruginosa, and Staphylococcus aureus. From the inhibition results these compounds have emerged as compelling alternatives to traditional antibiotics, offering a promising solution to combat the rise of antibiotic resistance. The study

confirms that the mixed metal oxides improve gas detection capabilities, opening up possibilities for improved and more advanced gas sensor materials.

Acknowledgments

The authors thank the Principal, Management, Head, staff members of V. O. Chidambaram College, Tuticorin to encourage the completion of the research work.

REFERENCES:

[1] B, Mughal, S.Z.J, Zaidi, X, Zhang, S.U, Hassan, Applied Sciences., **2021**, 11(6), p.2598.
[2] A, Selmani, D, Kovačević, K, Bohinc, Advances in Colloid and Interface Science., **2022**, 303, p.102640.
[3] A.K, Arora, V.S, Jaswal, K, Singh, R, Singh, Oriental Journal of Chemistry., **2016**, 32(4), p.2035.
[4] S, Stankic, S, Suman, F, Haque, J, Vidic, Journal of nanobiotechnology., **2016**, 14(1), pp.1-20.
[5] T, Takai, A, Shibatani, Y, Asakuma, A, Saptoro, C, Phan, Chemical Engineering Research and Design., **2022**, 182, pp.714-718.
[6] E, Gabano, M, Ravera, Molecules., **2022**, 27(13), p.4249.
[7] Q, Saleem, M, Torabfam, T, Fidan, H, Kurt, M, Yuce, N, Clarke, M.K, Bayazit, ACS Sustainable Chemistry & Engineering., **2021**, 9(30), pp.9988-10015.
[8] A.A, Aboud, H, Al-Kelesh, W.M, El Rouby, A.A, Farghali, A, Hamdedein, M.H, Khedr, Journal of materials research and technology., **2018**, 7(1), pp.14-20.
[9] T.D, Chu, D.T, Quach, X.T, Nguyen, T.S, Nguyen, D.T, Pham, D.H, Kim, Journal of Magnetics., **2020**, 25(1), pp.1-7.
[10] Z, Wang, S, Liu, X, Cao, S, Wu, C, Liu, G, Li, W, Jiang, H, Wang, N, Wang, W, Ding, Ceramics International., **2020**, 46(10), pp.15333-15341.
[11] V, Pathak, P, Lad, A.B, Thakkar, P, Thakor, M.P, Deshpande, S, Pandya, Results in Surfaces and Interfaces., **2023**, 11, p.100111.
[12] X, Cao, S, Zhao, S, Yan, J, Hu, Y, Dan, Journal of Renewable Materials., **2020**, 8(11), pp.1443-1472.
[13] A, Younis, D, Chu, S, Li, Funct. Nanomater., **2016**, 3, pp.53-68.
[14] V, Chikan, E.J, McLaurin, Nanomaterials., **2016**, 6(5), p.85.
[15] G, Eranna, Metal oxide nanostructures as gas sensing devices., CRC press; **2011**, Dec 19.
[16] M, Kareem, A, Suhad Hamdan, International Academic Journal of Science and Engineering., (2022), 9(2454-3896):37-45
[17] S, Mahajan, S, Jagtap, Applied materials today., **2020**, 18, p.100483.
[18] W, Buraso, V, Lachom, P, Siriya, P, Laokul, Materials Research Express., **2018**, 5(11), p.115003.
[19] R, Álvarez-Asencio, R.W, Corkery, A, Ahniyaz, RSC advances., **2020**, 10(25), pp.14818-14825.
[20] J, Zhang H, Chen, T, Wu, Faguang Xuebao, Chinese Journal of Luminescence.,**(2019)**.
[21] S, Bagheri, I, Khalil, N.M, Julkapli, Journal of Rare Earths., **2021**, 39(2), pp.129-139.
[22] K.K, Babitha, A, Sreedevi, K.P, Priyanka, B, Sabu, T, Varghese, Indian Journal of pure & applied physics., **2015,** 53(9), pp. 596-603.
[23] A, Gupta, K, Kushwah, S, Mahobia, P, Soni, V.V.S,Murty, International Journal of Innovative Technology and Exploring Engineering., **(2019).**
[24] T, Divya, C, Anjali, K.R, Sunajadevi, K, Anas, N.K, Renuka, Journal of Solid State Chemistry., **2021**, 300, p.122253.
[25] M, Nyoka, Y.E, Choonara, P, Kumar, P.P, Kondiah, V, Pillay, Nanomaterials., **2020**, 10(2), p.242.
[26] J.O, Tijani, M.M, Ndamitso, A.S, Abdulkareem, International Nano Letters., **(2021)**.
[27] K, Sharmila, V.A, Kamat, K, Swaroop, H.M, Somashekarappa, AIP Conferenc Proceedings., **2019**, October, (Vol. 2162, No. 1).
[28] B, Shirley, E, Jarochowska, Facies., **2022**, 68(2), p.7.
[29] Z.S, Duma, T, Sihvonen, J, Havukainen, V, Reinikainen, S.P, Reinikainen, Micron., **2022**, 163, p.103361.
[30] B, Lewczuk, N, Szyrynska, Animals., **2021**, 11, 3390.
[31] H, Bi, L.X, Zhang, Y, Xing, P, Zhang, J.J, Chen, J, Yin, L.J, Bie, Sensors and Actuators B: Chemical., **2021**, 330, p.129374.
[32] C.S, Kumar, M.M, Singh, R, Krishna, Advanced Materials Characterization: Basic Principles, Novel Applications, and Future Directions., CRC Press, **2023**.
[33] I, Rousso, A, Deshpande, Viruses., **2022**, 14(3), p.648.
[34] N.R, Stradiotto, H, Yamanaka, M.V.B, Zanoni, Electrochemical sensors., **2003**,
[35] J.S, Niu, I.P, Liu, K.H, Chen, J.H, Tsai, W.C, Hsu, W.C, Liu, Sensors and Actuators B: Chemical., **2022**, 369, p.132241.
[36] N, Elgrishi, K.J, Rountree, B.D, McCarthy, E.S, Rountree, T.T, Eisenhart, J.L, Dempsey, Journal of chemical education., **2018**, Feb 13;95(2):197-206.
[37] W, Shan, F, Liu, H, He, X, Shi, C, Zhang, Chemical Communications., **2011,** 47(28):8046-8.
[38] E, Fazio, S, Spadaro, C, Corsaro, G, Neri, S.G, Leonardi, F, Neri, N, Lavanya, C, Sekar, N, Donato, G, Neri, Sensors., **2021**, Apr 3;21(7):2494.
[39] Q, He, B, Wang, J, Liang, J, Liu, B, Liang, G, Li, Y, Long, G, Zhang, H, Liu, Materials Today Advances., **2023**, Mar 1;17:100340.
[40] I, Tsykhanovska, O, Stabnikova, S, Gubsky, Materials Proceedings., **2022**, Apr 22;9(1):2.
[41] S, Gurusamy, K, Krishnaveni, M, Sankarganesh, R.N, Asha, A, Mathavan, Journal of Molecular Liquids., **2022**345, p.117045.
[42] A, Happy, M, Soumya, S.V, Kumar, S, Rajeshkumar, R.D, Sheba, T, Lakshmi, V.D, Nallaswamy, Biophysics Reports., **2019**, Mar 1;17:208-11.

[43] C, Sun, X, Wang, J, Dai, Y, Ju, International Journal of Molecular Sciences., **2022**, Sep 26;23(19):11348.